IEEE Access
Multidisciplinary | Rapid Review | Open Access Journal

Received February 15, 2022, accepted March 25, 2022, date of publication March 30, 2022, date of current version April 8, 2022.

Digital Object Identifier 10.1109/ACCESS.2022.3163300

MILP-Based Service Restoration Method Utilizing Both Existing Infrastructure and DERs in Active Distribution Networks

MI-GON CHOI, (Student Member, IEEE), JOON-HO CHOI, (Senior Member, IEEE), SANG-YUN YUN, AND SEON-JU AHN, (Member, IEEE)

Department of Electrical Engineering, Chonnam National University, Buk-gu, Gwangju 61186, South Korea

Corresponding author: Seon-Ju Ahn (sjahn@chonnam.ac.kr)

This work was supported in part by the National Research Foundation of Korea (NRF) Grant funded by the Korean Government through the Ministry of Science and ICT (MSIT) under Grant 2021R1F1A1047729, and in part by the Regional Innovation Strategy (RIS) through NRF funded by the Ministry of Education (MOE) under Grant 2021RIS-002.

ABSTRACT This study proposes a service restoration method that utilizes the distributed energy resources (DERs) as the control measures as well as the existing infrastructure of the distribution system. The existing infrastructure includes switching operations, load shedding, and tap operations of the on-load tap changers (OLTCs). In addition, the DERs include reactive power control of the distributed generation (DG), charge/discharge of the energy storage system (ESS), and intentional islanding operation using the black-start function of the ESS. For this purpose, the following model is applied to the optimization problem based on mixed-integer linear programming. First, a linear constraint considering the voltage drop due to the impedance of the main transformer is used for practical application of an OLTC. Next, a linear constraint is formulated for grid code-based DG reactive power control. In addition, constraints for the ESS are defined. Here, the radiality constraints are formulated to distinguish the grid-connected and islanding operation modes based on the location and state of the ESS. Finally, simulations of the application of the control measures conducted on a 150-node test system, designed based on the data of the actual system in Korea, are conducted and the results are analyzed to verify the proposed method.

INDEX TERMS Service restoration, distributed energy resource, energy storage system, radiality, intentional islanding.

NOTATION

The notations used in this paper are as follows:

SETS

T_{repair}	Whole time for service restoration.
L_{out}	Loads in the unfaulty section.
sw_{cl}	Switches initially in closed state.
sw_{op}	Switches initially in open state.
C_{tap}	On-load tap changers installed in the system.
DG	DGs installed in the system.
ESS	ESSs installed in the system.

PARAMETERS

w_k	Weighting factor of objective function k.
w_i^l	Weighting factor of load i for priority.
S_{ij}^{max}	Maximum capacity of branch ij (MVA).
S_{ij}	Radius of n polygon.
a_{ij}^{min}	Minimum tap ratio of OLTC ij.
Δa_{ij}	Tap ratio step of OLTC ij.
tap_{ij}^{max}	Maximum value of OLTC tap.
N_{ij}	Number of binary variables to represent the tap of OLTC ij.
P_i^{rate}	Rated capacity of DG i (kW).
S_e^{max}	Maximum output of ESS e (kVA).
U^{min}	Square of minimum operational voltage (p.u).
U^{max}	Square of maximum operational voltage (p.u).
U^{ESS}	Square of voltage set point of ESS in intentional islanding mode (p.u).
$P_{i,t}^l$	Amount of load i at time t (kW).

The associate editor coordinating the review of this manuscript and approving it for publication was Ning Kang.

$P^{dg}_{i,t}$ Active power output of DG i at time t (kW).
$E_{e,1}$ Initial residual energy of ESS e.
E^{ini}_{e} Initial energy rate of ESS e.
E^{rate}_{e} Rated energy of ESS e.
η_c Charging efficiency of ESS.
η_d Discharging efficiency of ESS.
Δt Time variation of one step.

CONTINUOUS VARIABLES

$tap_{ij,t}$ tap value of OLTC ij at time t.
$Q^{dg}_{i,t}$ Reactive power of DG i at time t (kVar).
$P^{e}_{i,t}$ Active power of ESS i at time t (kW).
$Q^{e}_{i,t}$ Reactive power of ESS i at time t (kVar).
$P^{br}_{ij,t}$ Active power flow of branch ij at time t (MW).
$Q^{br}_{ij,t}$ Reactive power flow of branch ij at time t (MVar).
$U_{i,t}$ Square of voltage of node i at time t (p.u).
$a_{ij,t}$ Tap ratio of OLTC ij at time t.
$tap^{ch}_{ij,t}$ Changed Tap value of OLTC ij at time t.
$F_{ij,t}$ Fictitious load flow of branch ij at time t.
$E_{e,t}$ State of charge for ESS e at time t.

BINARY VARIABLES

n_i State of node i.
b_{ij} State of branch ij.
b^{sw}_{ij} State of switch ij.
$\lambda_{ij,n,t}$ Binary variable to represent the tap OLTC ij at time t.
$n^{dg'}_{i,t}$ State of the first reactive power range for DG i at time t.
$n^{dg''}_{i,t}$ State of the second reactive power range for DG i at time t.
$n^{dg'''}_{i,t}$ State of the third reactive power range for DG i at time t.
$r^{l}_{i,t}$ State of load i at time t.
$r^{s}_{i,t}$ State of source i at time t.
$n^{c}_{e,t}$ Charging state of ESS e at time t.
$n^{d}_{e,t}$ Discharging state of ESS e at time t.

I. INTRODUCTION

In modern society, continuous economic growth demands high-quality power supply. Service restoration (SR) is one of the most important operational methods of electric power companies for improving the quality and reliability of the power supply. The process re-energizes nonfaulty sections experiencing power outages during isolating the fault location. During this process, system constraints, such as thermal capacity and voltage of the adjacent feeder, applied to the non-faulty sections should be examined. The existing distribution system infrastructure, such as switches and on-load tap changers (OLTCs), can be utilized for satisfying the grid constraints by network reconfiguration and voltage control. In addition, control capability of inverter-based distributed generations (DGs), such as photovoltaics (PVs) and wind turbines (WTs), are utilized. An energy storage system (ESS) can also restore the loads by supporting active and reactive power and forming a microgrid (MG) using the black-start function. Here, PVs, WTs, and ESS are included in distributed energy resources (DERs) [1].

Several SR-related studies have been conducted using various methods. Expert systems and heuristic algorithm-based studies derived rule-based solutions for SR according to the objective of studies [2], [3]. Studies using graph theory mainly focused on increasing the derivation speed by removing candidates that cannot be solutions when determining the final topology of a system considering the switching operation and MG composition [4], [5]. Methods using meta-heuristic algorithms were developed considering the SR as a complex problem composed of multiple objectives and constraints and that a long time is required to derive a solution on the large scale of the network [6], [7]. Therefore, the above studies aimed to obtain a reasonable solution rapidly instead of an optimal solution that requires a long computation time. Multiagent-based research aimed to automatically implement SR in case of a fault by exchanging the information possessed by agents via communication in a decentralized architecture composed of agents with specific functions defined for each component [8], [9]. Also, the characteristics of components in distribution networks were considered. Sharma *et al.* reflected the islanding operation of the DG and vehicle-to-grid characteristics for electric vehicles [8]. In addition, they considered the uncertainty of the load and the DG [9].

Methods using mathematical programming aimed to obtain optimal SR solutions under multi-objective and multi-constraint conditions in the recently developed powerful computing environments by reflecting the features of the DERs as well as the existing infrastructure [10]–[23]. These works are directly related to the proposed method. Popovic *et al.* dealt with a mixed-integer problem in which the load variability was expressed by the Fuzzy algorithm [10]. Khushalani *et al.* solved the SR problem based on an unbalanced distribution system model by mixed-integer nonlinear programming (MINLP) and compared its speed and feasibility by defining a switch pair [11]. Romero *et al.* converted an existing MINLP problem into a mixed-integer second-order cone programming (MISOCP) problem and compared their speed performance in obtaining the solution [12]. However, these studies only considered the switching operation and the load without the features of the DERs. In [13], the switching operation was first calculated by mixed-integer linear programming (MILP) for an optimization problem constructed by linearizing the quadratic term of the line capacity of the power flow. Second, the load shedding (LS) amount was recalculated by nonlinear programming. To deal with the uncertainty caused by the load or the DG, Chen *et al.* modeled an optimization problem defining the load and DG fluctuation as an objective function for mixed-integer quadratic constraint programming and compared the SR results in terms of the fluctuation [14].

Additionally, in [15], an optimization model assuming the worst-case scenario was modeled by MILP to supplement the uncertainty treatment. López *et al.* modeled an optimization problem for calculating the necessary switching sequence in case of SR or operation interruption by MINLP [16]. Although the above studies included the functions of the DG in addition to the switching operation and the load, their solutions might lead to unnecessary control because of disregarding the load and DG profiles. In [17], the power flow constraint was modeled assuming a time-dependent load and DG profile based on predicted data. Under MINLP, the objective function was to maximize the gain in electricity trading in a normal condition and minimize the LS in an emergency condition. In addition, in an emergency, the MG zone was created to minimize the effect of a secondary fault. In [18]–[23], MILP-based SR optimization problems were modeled considering the dynamic state. A load model considering cold-load pickup (CLPU) after a fault in the MG was used in the optimization model to obtain the sequential SR results of the network [18]. This concept was extended to an unbalanced system [19], and the dynamic characteristics of inertia-based DG systems were reflected in the optimization model in the MG generation [20]. Additionally, switch operation time considering auto and manual switch was dealt with as well as several MG compositions. Also, SR method was modeled as variable time step and fixed-time step model and compared between the results from two models in [21]. Also, Song *et al.* dealt with time variation and uncertainty of CLPU in SR problem using MILP [22]. Although these methods dealt with the DG and load profiles and the dynamic characteristics of the DERs, they mainly focused on the MG configuration and did not consider OLTC control on the substation side.

In contrast, [23] included OLTC control and reactive power control of the PV system as well as the switching operation and LS in the SR problem using MISOCP. The amount of control was analyzed based on the addition of control measures. However, this method did not utilize additional functions of the DERs, such as islanding operations.

To summarize, the existing studies related to SR can be classified into those utilizing existing infrastructure such as LS and switching operations and those considering the effects of the DG and the DERs such as the MG and islanding operations. The former studies analyzed the results of SR considering the impact of the DG, without utilizing the additional functions of the DERs. Conversely, the latter studies focusing on the MG configuration did not consider the impact of the existing infrastructure such as OLTCs. To solve this problem, Koutsoukis *et al.* proposed an SR method using the control features of the active distribution network based on MISOCP [23]. In [23], reactive power control of the PVs and OLTC control were further addressed. However, these measures are used for alleviating voltage violations. Islanding operation using the black-start function and charge/discharge of the ESS, which can alleviate the violation of the line capacity, were not considered.

In this paper, a comprehensive SR method based on MILP is proposed. It includes the functions of the existing infrastructure and maximally considers the DERs. The objective function of the proposed method is to minimize the LS amount, number of switching operations and OLTC tap operations, amount of reactive power of the PV, and amount of charge/discharge of the ESS based on time-dependent load and DG profiles. First, linear constraints [24] representing the voltage drop of the distribution line for the main transformer (MTr) are applied to mimic a realistic OLTC tap operation. Next, linear constraints for the reactive power control of the PVs based on a grid code [25] are proposed for MILP application. Finally, constraints related to radiality and voltage range for the ESS are proposed. These constraints enable the ESS to perform two roles depending on the location when the network for restoration is configured. Based on the interconnection location of the ESS, the ESS can provide voltage and capacity support in the area isolated by an islanding operation and assistance for line capacity and voltage violation by charge/discharge in the gird-connected area [26]–[28]. Because the distribution line must maintain radiality even when the ESS performs its role based on the location, modified constraints for virtual power flow and the operating voltage range are proposed to mirror this condition. To verify the proposed method, MATLAB-based simulation are conducted on a 150-node test system designed based on statistical data of the distribution network for Korea [29], and the results are analyzed.

The remainder of the paper is organized as follows. Section II describes proposed service restoration method, Section III presents the formulation of the optimization model, and Section IV explain the constraints related to ESS operation. Section V discusses the simulation results, and finally, conclusions are drawn in Section VI.

II. PROPOSED SERVICE RESTORATION METHOD

In this study, SR method including scheduling of control measures and ESS operation is proposed as shown in Fig. 1. First, OLTC tap, reactive power of DG, load shedding and ESS charge/discharge are scheduled during repair time after a fault occurs using the profile of load and DG. This ensures that the voltage and line capacity are within the grid constraints. Second, ESS operations according to their location are utilized. The major functions of an ESS that can be utilized in the SR process are mitigation of the line capacity and voltage violation by charge/discharge in grid-connected area and providing additional power supply in the area isolated by an intentional islanding operation using black-start function. There are several existing studies based on a mathematical problem utilizing intentional islanding mode as the control measure in SR. Firstly, the creation of multiple MG areas was dealt with, considering the reduction of secondary fault effect [17]. However, many switch operations are required for multiple MG creation, and it could take a long operation time after a fault occurs. Also, this study did not consider the grid-connected

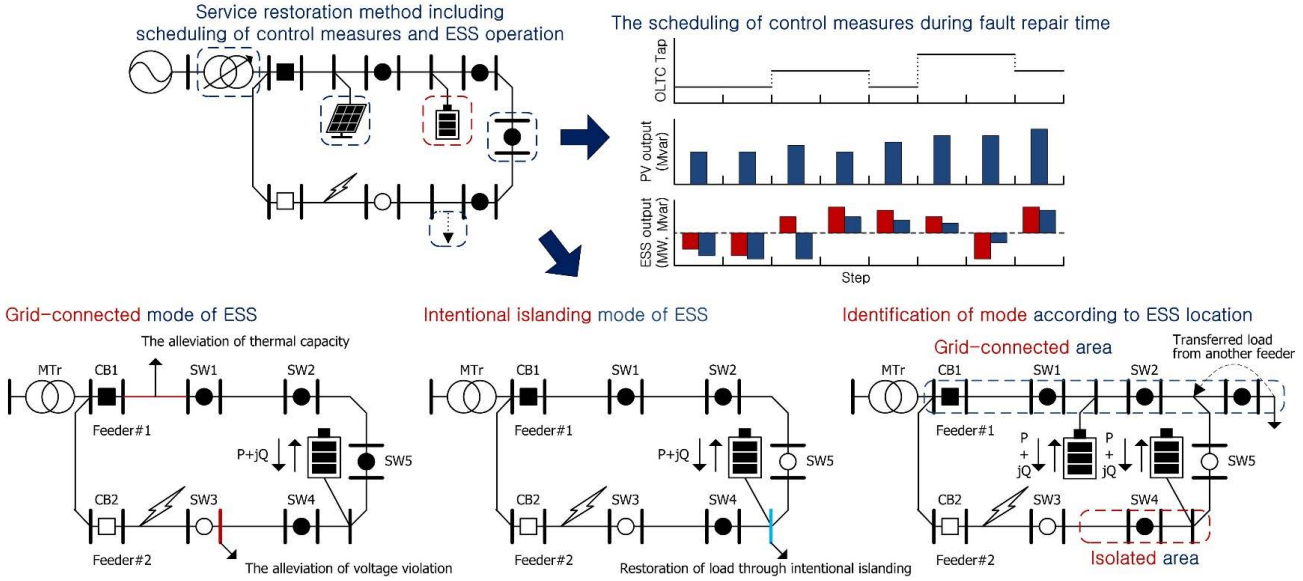

FIGURE 1. Proposed service restoration method.

operation of DERs in SR. Secondary, it was dealt with that the dynamic characteristics and switch operation time considering manual and auto switch in network configured with the grid-connected and isolated area [18], [21]. However, this study requires a destination of slack for a configuration of the isolated area from a substation. Accordingly, it is not possible to discriminate the grid-connected and intentional islanding mode of DERs according to a network condition for restoration.

In this study, the operation distinguishing the mode is included in SR according to network condition considering ESS as the black-start source with other control measures. Fig. 1 presents an example of ESS operation in SR process. It shows a simplified system including the interconnection of ESS according to the fault location. It is a two-feeder system and consists of one MTr, two circuit breakers (CBs) for each feeder and five switches (SWs). SW1-4 are normally closed, and SW5 is normally opened. The first presents a case when ESS is operated in a grid-connected mode. The fault occurred between CB2 of feeder#2 and SW3. The fault is cleared by CB2, and the fault location is isolated by opening SW3, following which the nonfaulty section of feeder#2 is restored by closing SW5. Because the load of feeder#2 is transferred to feeder#1, a more power flows in the red line than it normally would, which may violate the line capacity. In addition, the voltage drop may become severe under the weighted load, and a voltage drop violation may occur at the red node of restored feeder #2. When the state of charge (SoC) is sufficient, the ESS can alleviate the capacity violation by discharging the active power. Additionally, it can alleviate the voltage violation by supplying reactive power. The second shows a case when ESS is operated in an intentional islanding mode and used as black-start source. Depending on the SoC and load in an unfaulty section, the ESS can restore the load with no additional switch operation for transferring it to an adjacent feeder. In addition, the constant voltage is maintained by the voltage support at the installation point of the ESS in the blue node; therefore, the restored section can be operated in the normal voltage range. The third represents a case when multiple faults occurred. Another fault occurrence was assumed in another feeder. Therefore, some load was transferred to feeder#1. ESS located in feeder#1 is operated in a grid-connected mode. ESS located in feeder#2 is operated in and intentional islanding mode. In this case, ESSs should be operated in a proper mode according to their location. For reflecting these conditions, constraints for operation voltage range and radiality condition to distinguish the ESS operation are formulated in the proposed MILP-based SR problem.

III. MILP-BASED FORMULATION

A. OBJECTIVE FUNCTION

In this study, to include the effects of the DERs, an MILP-based optimization model is defined that considers the charging/discharging and islanding operation of the ESS and the control of the OLTC tap and reactive power control of the DG. The proposed optimization model is defined as follows:

$$min\, f = \sum_{k=1}^{6} w_k f_k \tag{1}$$

$$f_1 = -\sum_{t\in T_{repair}} \sum_{i\in L_{out}} w_i^l P_{i,t}^l \tag{2}$$

$$f_2 = \sum_{ij\in sw_{cl}} (1 - b_{ij}) + \sum_{ij\in sw_{op}} b_{ij} \tag{3}$$

$$f_3 = \sum_{t\in T_{repair}} \sum_{ij\in C_{tap}} |tap_{ij,t}^{ch}| \tag{4}$$

$$f_4 = \sum_{t\in T_{repair}} \sum_{i\in DG} |Q_{i,t}^{dg}| \tag{5}$$

$$f_5 = \sum_{t\in T_{repair}} \sum_{i\in ESS} |P_{i,t}^{e}| \tag{6}$$

$$f_6 = \sum_{t \in T_{repair}} \sum_{i \in ESS} |Q^e_{i,t}| \tag{7}$$

The objective function consists of six terms, as expressed in (1), and a weight is applied to each element. Equation (2) means the weighted amount of LS in the nonfaulty section during the repair time. The weighting factor (w^l_i) for each load is determined by its priority. Equation (3) represents the number of switch operations to form the configuration for SR. Equation (4) shows the number of OLTC tap operations of all steps during the repair time. Equation (5) represents the amount of reactive power control of the controllable DGs. Equation (6) and (7) show the amount of active and reactive power control of the ESSs, respectively. The terms expressed as absolute values in (4) – (7) are linearized by introducing the constraints presented in [23]. Weighting factor (w_k) can be determined based on the cost of each term, such as interruption cost of the shed loads, lifetime reduction cost of switches and OLTCs, and the compensation cost for utilizing the DERs [13].

B. CONSTRAINTS: POWER FLOW AND LINE CAPACITY LIMIT

Because this study uses MILP, a linear constraint is required. Therefore, simplified DistFlow is used. This equation is a linearly simplified by deleting the power loss. It is considered that the use of this formula is appropriate for the distribution system that consists of the short line length and the line type with small loss [18].

Additionally, the maximum capacity constraint for the line is expressed in (8). However, because it has a quadratic form, it needs to be linearized.

$$\left(P^{br}_{ij,t}\right)^2 + \left(Q^{br}_{ij,t}\right)^2 \le \left(S^{max}_{ij}\right)^2 \tag{8}$$

Equation (9) is obtained by linearizing (8) using a polygon-based linearization technique [30]. As the size of polygon increases, the computational burden will increase, but the loss of accuracy during the linearization process can be reduced. In this study, the equations with polygon size $n = 12$ are used. If the computation time is the critical issue in a large distribution network, a smaller polygon size can be used.

$$\begin{aligned}
&-\left(\sqrt{3}+2\right)\left(P^{br}_{ij,t}+S_{ij}\right)\\
&\le Q^{br}_{ij,t} \le -\left(\sqrt{3}+2\right)\left(P^{br}_{ij,t}-S_{ij}\right)\\
&\quad -P^{br}_{ij,t}-\left(\sqrt{3}+1\right)S_{ij}/2 \le Q^{br}_{ij,t}\\
&\le -P^{br}_{ij,t}+\left(\sqrt{3}+1\right)S_{ij}/2\left(\sqrt{3}-2\right)P^{br}_{ij,t}-S_{ij}\\
&\le Q^{br}_{ij,t} \le \left(\sqrt{3}-2\right)P^{br}_{ij,t}+S_{ij}-\left(\sqrt{3}-2\right)P^{br}_{ij,t}-S_{ij}\\
&\le Q^{br}_{ij,t} \le -\left(\sqrt{3}-2\right)P^{br}_{ij,t}+S_{ij}P^{br}_{ij,t}-\left(\sqrt{3}+1\right)S_{ij}/2\\
&\le Q^{br}_{ij,t} \le P^{br}_{ij,t}+\left(\sqrt{3}+1\right)S_{ij}/2\left(\sqrt{3}+2\right)\left(P^{br}_{ij,t}-S_{ij}\right)\\
&\le Q^{br}_{ij,t} \le \left(\sqrt{3}+2\right)\left(P^{br}_{ij,t}+S_{ij}\right)
\end{aligned} \tag{9}$$

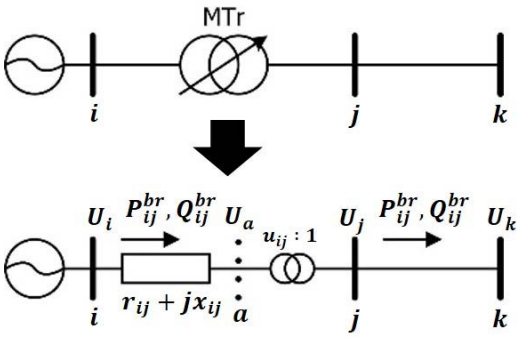

FIGURE 2. Diagram of linearized OLTC formulation.

S_{ij} for polygon n is calculated using (10).

$$S_{ij} = S^{max}_{ij}\sqrt{(2\pi/n)/\sin(2\pi/n)} \tag{10}$$

C. CONSTRAINTS: OLTC TAP CONTROL

An OLTC changes the voltage at the sending end of the feeder by adjusting the tap of the MTr [31]. In a previous study dealing with an OLTC in SR, the minimum voltage was set according to the OLTC control to 1.0 p.u., and the voltage drop due to the impedance of the MTr [23] was neglected. Therefore, this study reflects the linear constraints of the OLTC [24], which can consider the voltage drop caused by the impedance of the MTr. Fig. 2 represents the MTr as an impedance and the tap ratio of the OLTC. The voltage drop is due to the power flow in branch *i–j* and the internal impedance of the MTr. Simultaneously, the voltage adjustment according to the OLTC tap change should be reflected in node *j*. Therefore, a virtual node "*a*" is created between nodes *i* and *j*, and the voltage drop due to the MTr impedance is applied to branch *i–a*. In addition, the result of the voltage adjustment by changing the OTLC tap is applied to existing node *j*.

The equations for the OLTC tap control are as follows. Equation (11) expresses the voltage change based on the tap ratio on the secondary side of the transformer. Because the square of the voltage is used for linearization, the tap ratio should also be squared. Equation (12) expresses the tap ratio. Based on the minimum value of the tap ratio, the current tap ratio is calculated considering the current tap value.

$$U_{a,t} = a^2_{ij,t}U_{j,t} \tag{11}$$

$$\begin{aligned}
a_{ij,t} &= a^{min}_{ij} + \Delta a_{ij} tap_{ij,t},\\
0 &\le tap_{ij,t} \le tap^{max}_{ij}
\end{aligned} \tag{12}$$

Equation (13) expresses the current tap ratio and can be linearized using binary variable λ_{ij}. Equation (14) describes the constraint on the maximum tap value.

$$a_{ij,t} = a^{min}_{ij} + \Delta a_{ij}\sum_{n=0}^{N_{ij}} 2^n \lambda_{ij,n,t} \tag{13}$$

$$\sum_{n=0}^{N_{ij}} 2^n \lambda_{ij,n,t} \le tap^{max}_{ij} \tag{14}$$

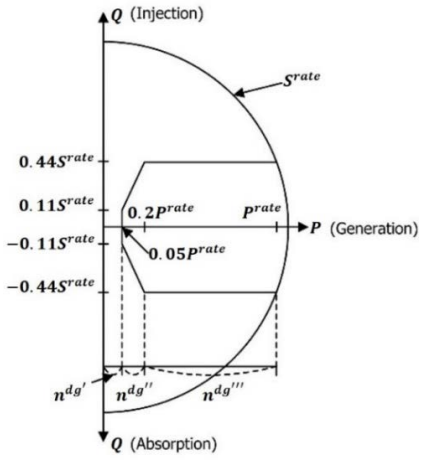

FIGURE 3. Range of reactive power control of DG.

Because $a_{ij,t}^2 U_{j,t}$ in (15) is nonlinear, it should be linearized by introducing new variables $d_{ij,t}$ and $y_{ij,n,t}$ as follows:

$$U_{a,t} = a_{ij}^{min} d_{ij,t} + \Delta a_{ij} \sum_{n=0}^{N_{ij}} 2^n y_{ij,n,t} \tag{15}$$

Equation (16) is used to calculate the final tap value with (13)–(15).

$$tap_{ij,t} = \sum_{n=0}^{N_{ij}} 2^n \lambda_{ij,n,t} \tag{16}$$

In this study, Δa_{ij} is set as 0.0125 and tap_{ij}^{max} is 16, representative of the typical OLTC controller used in Korea [32].

D. CONSTRAINTS: REACTIVE POWER CONTROL OF INVERTER

The reactive power control of the inverter is modeled based on category 2 of IEEE standard 1547-2018, as shown in Fig. 3 [25]. The output range of the reactive power is divided into three areas according to the active power output of the DG. To apply these ranges to MILP, the equation was linearized using big-M and three binary variables.

The areas are divided using (17)–(23) with binary variables $n_i^{dg'}$, $n_i^{dg''}$, and $n_i^{dg'''}$. For example, if the output of the DG inverter is in the range of (17), $n_i^{dg'}$ is set as "1," and the remaining binary variables $n_i^{dg''}$ and $n_i^{dg''}$ are set as "0" using (23). Therefore, the results of the reactive power range are obtained from (18), and the remaining range is not affected by big-M. In addition, the maximum capacity of each DG is selected using (15). In Fig. 3, the range of the reactive power is represented as a function of the rated capacity (S^{rate}). In (18), (20), and (22), the range of the reactive power is rewritten as a function of the rated active power (P^{rate}) by assuming S^{rate} is 1.1 times P^{rate} [23].

$$\begin{aligned} M\left(n_{i,t}^{dg'} - 1\right) &\le P_{i,t}^{dg} \\ &\le M\left(1 - n_{i,t}^{dg'}\right) + 0.05P_i^{rate} \end{aligned} \tag{17}$$

$$M\left(n_{i,t}^{dg'} - 1\right) \le Q_{i,t}^{dg} \le M\left(1 - n_{i,t}^{dg'}\right) \tag{18}$$

$$\begin{aligned} M\left(n_{i,t}^{dg''} - 1\right) + 0.05P_i^{rate} &\le P_{i,t}^{dg} \\ &\le M\left(1 - n_{i,t}^{dg''}\right) + 0.2P_i^{rate} \end{aligned} \tag{19}$$

$$\begin{aligned} M\left(n_{i,t}^{dg''} - 1\right) - 2.42P_{i,t}^{dg} &\le Q_i^{dg} \\ &\le M\left(1 - n_{i,t}^{dg''}\right) + 2.42P_{i,t}^{dg} \end{aligned} \tag{20}$$

$$\begin{aligned} M\left(n_{i,t}^{dg'''} - 1\right) - 0.2P_i^{rate} &\le P_{i,t}^{dg} \\ &\le M\left(1 - n_{i,t}^{dg'''}\right) + P_i^{rate} \end{aligned} \tag{21}$$

$$\begin{aligned} M\left(n_{i,t}^{dg'''} - 1\right) - 0.484P_i^{rate} &\le Q_{i,t}^{dg} \\ &\le M\left(1 - n_{i,t}^{dg'''}\right) + 0.484P_i^{rate} \end{aligned} \tag{22}$$

$$n_{i,t}^{dg'} + n_{i,t}^{dg''} + n_{i,t}^{dg'''} = 1 \tag{23}$$

E. CONSTRAINTS: NODE AND BRANCH

For the proposed SR method, the constraints on the nodes and lines should be defined. For example, when a line is electrically connected, both nodes must also be connected and vice versa. Even if both nodes are electrically connected, the switch is not connected if the state is "open." If at least one of the two nodes is electrically connected, the line must be connected, and the opposite node of the two sides must also be connected as shown in (24).

$$b_{ij}^{br} = n_i = n_j \tag{24}$$

Equations (25) and (26) are the constraints on the switch. Even if both nodes are electrically connected, they may or may not be connected depending on the open/close state of the switch.

$$b_{ij}^{sw} \le n_i, \tag{25}$$

$$b_{ij}^{sw} \le n_j \tag{26}$$

Additionally, it is assumed that the load and source nodes restored in the previous step must keep connected, as expressed in Eq. (27) and (28).

$$r_{i,t}^{l} \ge r_{i,t-1}^{l}, \tag{27}$$

$$r_{i,t}^{s} \ge r_{i,t-1}^{s} \tag{28}$$

IV. CONSTRAINTS FOR ESS OPERATION

In this paper, ESS operation is included in SR as a control measure. ESS operation is divided into grid-connected and intentional islanding modes. These modes should be appropriately determined according to ESS's location and network condition. For applying these conditions to the SR problem, modified constraints for operational voltage range and radiality are required as well as ESS operation.

A. OPERATIONAL VOLTAGE RANGE

A distribution system must be operated within a specific voltage range for stable power supply. Therefore, the squared voltage of all nodes should be within the minimum and maximum limit values, i.e., U^{min} and U^{max}. Because it is assumed that the ESS can operate as an intentional islanding mode, the constraints regarding the voltage of the ESS node should be carefully defined. When the ESS is in a grid-connected operation, the voltage at the ESS node is determined according to the power flow, and the squared voltage value should be within U^{min} and U^{max}. In contrast, if the ESS is operated as an intentional islanding mode, the ESS node voltage should be maintained at a predefined reference value. In this case, the ESS node acts as a slack node, and the voltages of the other nodes in the islanded area are determined based on the ESS node voltage and the power flow. In this study, the ESS node voltage is set as 1.0 p.u. when it is operated as an intentional islanding mode. Equations (29) and (30) express the voltage constraints of the ESS node that satisfies both operation modes by introducing a binary variable n_{em}. The value of n_{em} is 1 when the ESS is a black-start source.

$$U^{min} n_e + \left(U^{ESS} - U^{min}\right) n_{em} - U_e \leq 0 \tag{29}$$

$$-U^{max} n_e - \left(U^{ESS} - U^{max}\right) n_{em} + U_e \leq 0 \tag{30}$$

B. CONSTRAINTS: RADIALITY

A distribution network after a switching operation for SR should maintain the radial structure. Therefore, various constraints were applied in the previous SR studies. However, because the radial conditions vary depending on the role of the ESS, the constraints should be modified. Equation (31) presents the basic radiality condition, which is that the sum of the number of nodes and the number of slack (root) nodes is equal to the number of branches. If the ESS acts as a black-start source, it should be considered as a slack node. Therefore, binary variable n_{em} is added to the right term in the equation. If there is no islanded area, all variables n_{em} are zero; thus, Equation (31) becomes the same as the conventional constraint. In [33], it was shown that the constraint in (31) alone may not satisfy the radiality condition if DERs are present in the network. To solve this problem, the virtual power flow equation of a fictitious demand is defined as in (32). This constraint is applied to all nodes, except the slack node. In this study, because the ESS node can be either a load node or a slack node according to the operation mode, the modified constraints written in (33) and (34) are proposed.

$$\sum n_i - \sum b_i = \sum r_i^s + \sum n_{em} \tag{31}$$

$$\sum_{ki \epsilon ke} F_{ki,t} + n_i = \sum_{ij \epsilon ej} F_{ij,t} \tag{32}$$

$$-n_e + (1 - M)\, n_{em} \leq \sum F_{ke} - \sum F_{ej} \tag{33}$$

$$n_e - (1 + M)\, n_{em} \leq -\sum F_{ke} + \sum F_{ej} \tag{34}$$

C. ESS OPERATION

The general constraints for ESS operation are used [16]. Equation (35) allows only one of charging or discharging when the ESS node is electrically connected. Equation (36) is the initial SoC and is calculated based on the rated capacity of the ESS. In Equation (37), the SoC of the current step is calculated when the ESS is operating. Losses due to efficiency and elapsed time are applied during charging/discharging.

$$n_{e,t}^c + n_{e,t}^d \leq n_e \tag{35}$$

$$E_{e,1} = E_e^{ini} E_e^{rate} \tag{36}$$

$$E_{e,t} = E_{e,t-1} + \eta_c P_{e,t}^c \Delta t - \frac{1}{\eta_d} P_{e,t}^d \Delta t \tag{37}$$

V. CASE STUDIES

Fig. 4 shows the 150-node test system used in the simulation study to verify the proposed SR method. The test system topologies and parameters are based on actual distribution system data of Korea Electric Power Corporation (KEPCO) [29]. The amount of LS and the control results during the SR were analyzed based on the applicable control measures in four scenarios with different fault locations and DG and load profiles. It was assumed that 2 h are required to repair the fault in this study. Therefore, eight steps of 15-min interval loads and DG profile data are used as the input for each scenario. The fault locations are marked in Fig. 4.

The test system consists of two substations and four feeders. The line type is ACSR 160 mm^2, whose impedance is 0.1823 + j0.3901 Ω/km, and the maximum capacity in emergency condition is 14 MVA. The rated voltage of the system is 22.9 kV, and the range of the operating voltage is 0.96–1.02 p.u. The lengths of feeder #1–#4 are 5 km, 10 km, 15 km, and 30 km, respectively. The load capacity is varied from 100 kW to 1000 kW according to type, such as residential, commercial, and industrial load. The total rated capacity of the load in the four feeders are 10 MVA, 10 MVA, 9.2 MVA, and 9 MVA, respectively, and the 24 h load profiles of the four feeders are shown in Fig 5 (a).

All DGs installed in the system are assumed to be PV generators with the output profile as shown in Fig 5 (b).

The priority of the six terms in the objective function is determined as described in Section III.A, and the value of the weighting factors (ω_k) are set as listed in Table 1. The values for $\omega_1 \sim \omega_3$ were determined based on actual cost [29], [34]. In the case studies, $\omega_4 \sim \omega_6$ were set to zero assuming that the DERs are owned by the utility and that financial compensation is not required to utilize them. In addition, the weighting factor of each load (ω_i^l) to determine the priority of the shedding is set according to its capacity as listed in Table 2.

Table 3 summarizes the locations and capacity of the PVs in the test system. The PV output in the faulted sections is assumed to be zero during the first step and follows the profile if the PV-connected node is restored during the SR process.

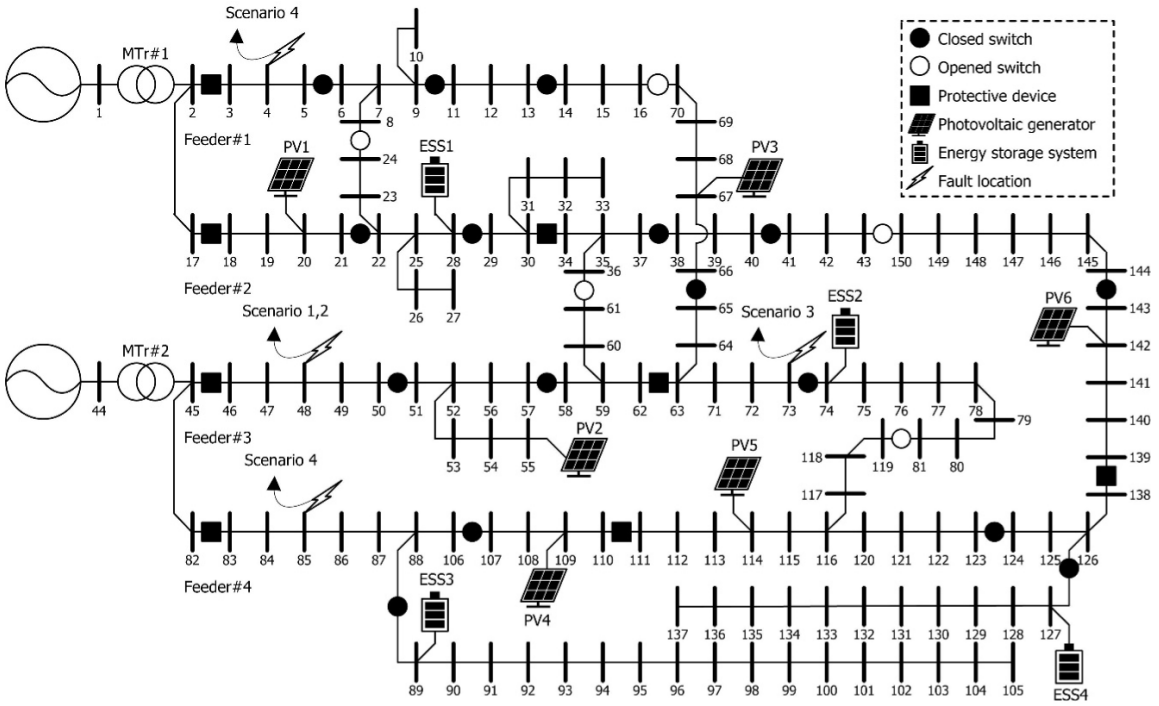

FIGURE 4. Schematic of 150-node test system.

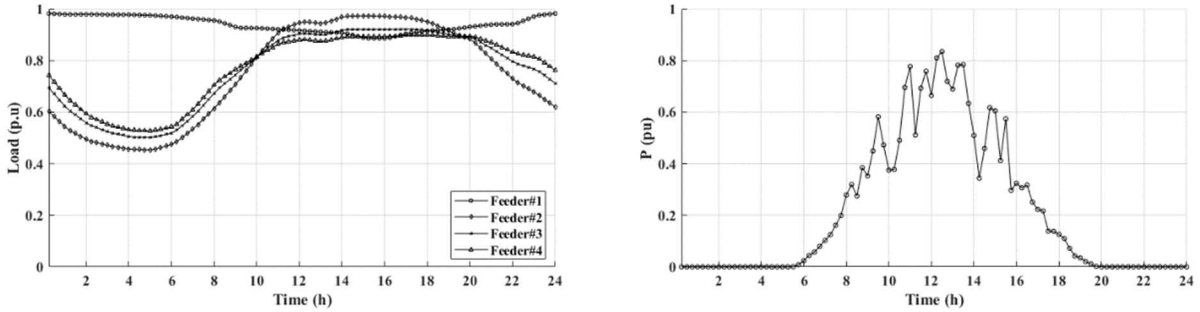

FIGURE 5. Profiles for simulation: (a) Load profiles, (b) PV profiles.

TABLE 1. Weighting factor of each term in objective function (krw).

Parameter	ω_1	ω_2	ω_3	ω_4	ω_5	ω_6
Value	3,500/ kWh	4,250/ switching	1,800/ tap	0/ MVarh	0/ kWh	0/ MVarh

TABLE 2. Weighting factor of load for determining priority of shedding.

Load capacity (S_i^l)	$S_i^l \leq 200$ kVA	200 kVA $< S_i^l \leq 500$ kVA	500 kVA $< S_i^l$
Weighting factor (ω_i^l)	1	3	5

Four ESSs are installed in the system, and the location and parameters of the ESSs are summarized in Table 4. It is assumed that all ESSs have the black-start function, and the SoC range of each ESS is between 30% and 90%.

TABLE 3. PV parameters for test system.

PV number	Feeder	Node	Rated capacity (kW)
PV1	#2	20	1,500
PV2	#3	55	2,000
PV3	#3	67	2,500
PV4	#4	109	1,500
PV5	#4	114	2,500
PV6	#4	142	2,500

A. SCENARIO 1 RESULTS

Scenario 1 was designed to analyze the effect of the OLTC control and the ESS, which was operated in the grid-connected mode. The load profile of 20–22 h was selected when the load was heavy but there was no PV output.

TABLE 4. ESS parameters for test system.

ESS number	Feeder	Node	Rated capacity (kWh)	S_e^{max} (kVA)
ESS1	#2	28	2,000	1,000
ESS2	#3	74	2,000	1,000
ESS3	#4	89	1,500	750
ESS4	#4	127	1,500	750

TABLE 5. Control measures applied in four cases of scenario 1.

Cases	SW operation and LS	OLTC tap control	Reactive power control of DG	ESS operation
Case 1-1	O	X	X	X
Case 1-2	O	O	X	X
Case 1-3	O	O	X	O (SoC_e^{ini} = 30%)
Case 1-4	O	O	X	O (SoC_e^{ini} = 90%)

TABLE 6. Amount of LS for Case 1-1 (kW).

Node	53	54	60	61	64	73
Step 1	437.6	486.5	312.8	265.3	176.9	81
Step 2	442.4	491.8	316.2	268.3	-	78.6
Step 3	447.3	497.2	319.7	271.2	-	-
Step 4	452.1	502.5	-	274.1	-	-
Step 5	455.2	506	-	-	-	-
Step 6	456.3	507.2	-	-	-	-
Step 7	457.5	508.5	-	-	-	-
Step 8	-	509.8	-	-	-	-

It was assumed that the fault occurred between CB 45-46 and SW 50-51 of feeder#3 and was isolated by operating the CB and SW. The OLTC taps of both MTrs were adjusted to 7 in the pre-fault state to compensate for the severe voltage drop caused by the heavy load. Four cases were simulated according to the applicable control measures and the initial SoC of the ESS (SoC_e^{ini}), as summarized in Table 5.

Case 1-1: Seven switches were operated: 16-70 (NO), 36-61 (NO), 43-150 (NO), 81-119 (NO), 40-41 (NC), 65-66 (NC), 73-74 (NC). In this case, most of the loads of feeder #3 were transferred to feeders #1, #2, and #4. However, some of the loads could not be restored because there was no additional control method except the switch operation. Table 6 lists the amount of LS of each node at each time step. For example, the load at node 60 can be restored from step 4, whereas the loads at node 54 are shed during the entire repair time. The minimum voltage was 0.96 p.u. at node 51 from step 1 to step 7, and the maximum power flow was 11.21 MVA in branch 17-18 at step 1. Therefore, in this case, the critical constraint for LS is the minimum voltage limit.

Case 1-2: Three switches were operated: 36-61 (NO), 43-150 (NO), 37-38 (NC). The OLTC tap of both MTrs was changed from 7 to 6 in the first step, and this tap was maintained for the remainder of time. In this case, all loads were restored. The minimum voltage was approximately 0.96 p.u. at node 38 at step 1, and the maximum power flow was 13.58 MVA in branch 17-18. Compared with Case 1-1, the voltage violation was alleviated by the OLTC tap control; therefore, no LS occurred, and the number of switch operations was reduced from 7 to 3.

Case 1-3: Three switches were operated: 36-61 (NO), 43-150 (NO), 37-38 (NC). In this case, the taps of both MTrs were not changed. Because the initial SoC of the ESSs were 30%, they could not provide the enough active power; however, the ESSs in feeders #2, #3 and #4 supported the reactive power to resolve the voltage problem. The minimum voltage was 0.96 p.u. at node 38, and the maximum power flow was 13.90 MVA in branch 17-18. Compared with Case 1-2, the number of switching operation was the same, but the number of OLTC tap operation decreased with the reactive power support from the ESSs. In summary, the number of operations of the control measure for alleviating the voltage violation was reduced.

Case 1-4: In this case, all loads were restored by only operating SW 36-61 (NO). The tap of MTr#1 was changed to 6 at step 1, whereas that of MTr#2 was not changed. The minimum voltage was 0.96 p.u. at node 81 for all steps, and the maximum power flow was 13.90 MVA in branch 17-18 at step 1. Because the ESSs discharged energy as well as supported the reactive power, the maximum power flow in feeder#2 was maintained below the limit although all loads of feeder#3 were transferred. Fig. 6(a) shows the active power of ESS1 in feeder#2 for Case 1-4. ESS1 discharged the energy based on the load profile of 20–22 h because the SoC was sufficient. Therefore, all load of feeder#3 could be transferred to feeder#2 without violating the line capacity limit. Fig. 6(b) compares the reactive power outputs of ESS2 for Cases 1-3 and 1-4. In Case 1-3, the loads of feeder#3 were transferred to feeder#4. Because the voltage drop of feeder#4 was larger than that of feeder#2 in Case 1-4, more reactive power was supported by ESS1 to mitigate the voltage drop than in Case 1-3.

The results of Scenario 1 are summarized in Table 7. No LS occurred when operating the OLTC tap, and the number of switching operation was also reduced. The addition of the ESS operation reduced the number of switching and OLTC tap operations by supplying sufficient energy.

B. SCENARIO 2 RESULTS

In Scenario 2, the SR results following addition of the control of the reactive power of the DGs and the ESS operation are analyzed for a fault occurring when the DGs generate power. The load profile of 16–18 h was selected when the load is heavy and the PV output is approximately 20% of the rated power. Table 8 summarizes four cases based on the applied control measures.

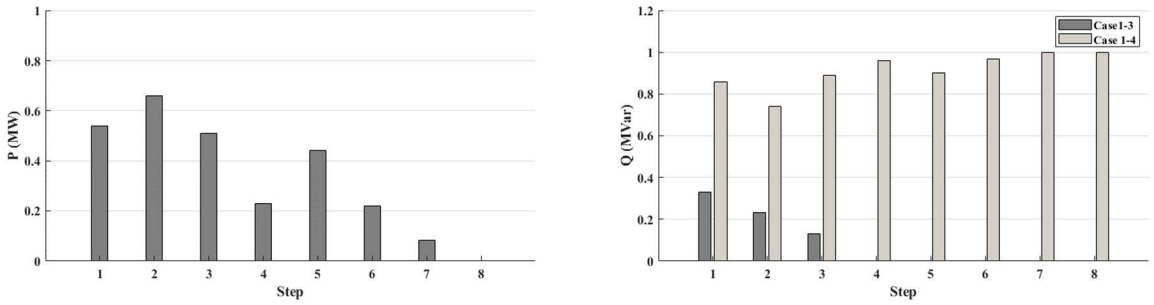

FIGURE 6. Comparison of outputs of ESS1 in Cases 1-3 and 1-4: (a) Active power output in Case 1-4, (b) Reactive power outputs in Cases 1-3 and 1-4.

TABLE 7. Summary of results of scenario 1.

Cases	Amount of LS (kWh)	OLTC Tap operations	Number of SW operations
Case 1-1	2456.5	-	7
Case 1-2	0	#1 1tap, #2 1tap	3
Case 1-3	0	-	3
Case 1-4	0	#1 1tap	1

TABLE 8. Control measures applied in four cases of scenario 2.

Cases	SW operation and LS	OLTC tap control	Reactive power control of DG	ESS operation
Case 2-1	O	O	X	X
Case 2-2	O	O	O	X
Case 2-3	O	O	O	O ($SoC_e^{ini} = 30\%$)

Case 2-1: Three switches were operated: 36-61 (NO), 43-150 (NO), and 37-38 (NC). The OLTC taps of both MTrs were changed from the 7 to 6 in the first step and maintained for the remaining. Also, all loads in the unfaulty section were restored through OLTC tap operation like Case 1-2. The minimum voltage was 0.96 p.u. at node 81, and the maximum power flow was 13.47 MVA at branch 17-18.

Case 2-2: All loads were restored like Case 2-1 by operating three switches: 36-61 (NO), 43-150 (NO), and 37-38 (NC). OLTC tap of MTr#1 was changed to 6 at step 1, whereas that of MTr#2 was not changed. The minimum voltage was 0.96 p.u. at node 38, and the maximum power flow was 13.49 MVA in branch 17-18. In summary, the number of OLTC tap operations was decreased because the DG systems supported the reactive power.

Case 2-3: All loads were restored by operating only one switch: 81-119 (NO). Also, the taps of the OLTCs were not changed. The minimum voltage was 0.96 p.u. at node 51, and the maximum power flow was 13.37 MVA in branch 82-83. In this case, all loads were restored with one switch operation because the reactive power for alleviating the voltage violation was sufficiently provided by the DGs and ESSs.

C. SCENARIO 3 RESULTS

Scenario 3 aims to verify the ESS operation as an intentional islanding operation in case of a single fault. The load and PV profile of 2-4 h was selected when the load was light; also, there was no PV output. Fault occurred between recloser 62-63 and SW, 73-74 of feeder#3. Therefore, the fault was isolated through the close of switches 73-74 and 65-66. Two cases with different ESSs' initial SoC are compared. The initial SoC in Case 3-1 is 30% and that of Case 3-2 is 90%. All the other control measures are applied the same in both cases.

Case 3-1: Two switches were operated: 16-70 (NO) and 81-119 (NO). The OLTC taps of both MTrs were not changed. Also, all loads were restored. There was no violation of operation voltage range and thermal capacity with no operation of other control measures because the loads in unfaulty section was small. In this case, the two unfaulty sections were created by the fault location. Therefore, two switches were operated when there was no energy in ESS.

Case 3-2: One switch operation: 16-70 (NO). The OLTC taps of both MTrs were not changed, and all loads were restored like Case 3-1. In contrast to Case 3-1, all loads were restored by only one switch operation. Because the energy in ESS2 was enough, the loads at nodes 75-81 were able to be restored with the intentional islanding operation of ESS2 and no operation of SW 81-119.

Fig. 7 shows the active/reactive power and SoC of ESS2 for the intentional islanding operation. ESS2 supplied the power to restore the loads in the isolated area to the maximum extent; thus, the SoC at the final step reached the minimum limit, i.e., 30%. In addition, the reactive power support of ESS2 allowed the node voltages in the isolated area to be maintained within the normal operating range.

D. SCENARIO 4 RESULTS

Scenario 4 aims to verify the ESS operation in case of multiple faults. The load and PV profiles were the same as those of Scenario 2. It was assumed that two faults occurred simultaneously. One fault occurred between

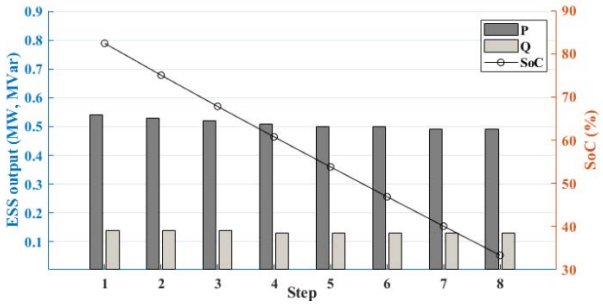

FIGURE 7. Active and reactive power and SoC of ESS2 in intentional islanding operation.

TABLE 9. Amount of LS for Case 4-1 (kW).

Node	138	143	144
Step 1	153.9	152.4	152.4
Step 2	154.8	153.2	153.2
Step 3	155.7	154.1	154.1
Step 4	156.5	154.9	154.9
Step 5	157.5	155.9	155.9
Step 6	158.8	157.2	157.2
Step 7	160	158.4	158.4
Step 8	161.3	159.6	159.6

CB 2-3 and SW 5-6 of feeder#1, and the other location was between CB 82-83 and SW 106-107 of feeder#4. Two cases are compared according to whether the ESS is operated. In both cases, all other control measures are applied.

Case 4-1: The ESSs were not operated in this case. Four switches were operated: 8-24 (NO), 16-70 (NO), 81-119 (NO), 13-14 (NC). The OLTC tap of MTr#1 was not changed, whereas that of MTr#2 was changed to 6 at step 1. However, the loads of nodes 90–105 were not restored because there was no interconnection switch for transferring this section load to other feeders when SW 88-89 was opened for fault isolation. In addition, some of the loads in the non-isolated area could not be restored due to the network limits, as summarized in Table 9. The minimum voltage was 0.96 p.u. at node 150, and the maximum power flow was 14.06 MVA in branch 17-18. The LS occurred in the nodes initially fed from feeder#4, whereas all loads in feeder#1 were restored because of the following reasons. First, the capacity of the loads of feeder#1 was larger than that in feeder#4; therefore, the weighting factor (ω_i^l) was also higher. Second, because the length of feeder#4 was long, the voltage drop incurred in restoring the loads of this feeder became severe.

Case 4-2: ESS operation was included in this case, and a total of two switches were operated: 16-70 (NO), 43-150 (NO). The OLTC taps of both MTrs were changed to 6. All loads listed in Table 9 could be restored by the discharge from ESSs. Moreover, a part of the loads in the isolated section could be restored with the intentional islanding operation of ESS3. In total, the amount of LS decreased from 2897.86 kWh of Case 4-1 to 1150.6 kWh. The minimum voltage was 0.96 p.u. at node 150, and the maximum power flow was 13.95 MVA in branch 45-46. ESS3 could restore some of the loads in the isolated area. Moreover, ESSs 1, 2, and 4 could relax the line capacity of feeders #2 and #3 to which the loads of feeders #1 and #4 were transferred. The ESSs could also reduce the amount of control of switch and OLTC tap operation. Finally, the results confirmed that the proposed SR formulation with modified radiality and voltage range constraints could simultaneously deal with ESS operations in both grid-connected and intentional islanding modes.

TABLE 10. Adjusted weighting factors (krw).

Parameter	ω_1	ω_2	ω_3	ω_4	ω_5	ω_6
Value	3,500/ kWh	4,250/ switching	1,800/ tap	2,700/ MVarh	50,000/ MWh	2,700/ MVarh

TABLE 11. Restoration results of scenario 1 with different weighting factors.

Cases	Switch operation	OLTC tap operation
Case1-3 (Base)	3	-
Case1-4 (Base)	1	#1 1tap
Case1-3 (Adjusted)	3	#1 1tap, #2 1tap
Case1-4 (Adjusted)	3	#1 1tap, #2 1tap

E. EFFECT OF WEIGHTING FACTORS

If the DERs are not owned by the utility, financial compensation may be required when using them for SR. In this case study, weighting factors $\omega_4 \sim \omega_6$ were set as shown in Table 10, assuming the ownership of the DERs are on the customer side [35] [36]. Table 11 summarizes the results of two simulations using different weighting factors $\omega_4 \sim \omega_6$ in the scenarios of Case 1-3 and 1-4. In the table, 'Base' means the results when $\omega_4 \sim \omega_6$ were set to zero, while 'Adjusted' represents the results when $\omega_4 \sim \omega_6$ of Table 10 were used. It was found that the utilization of OLTC or switch control have increased instead of utilizing the active/reactive power control of ESSs and DGs if compensation costs are incurred because DERs are not owned by the utility.

F. SUMMARY AND DISCUSSION

In this paragraph, the results of case studies are summarized and discussed. In scenario 1, the amount of control was reduced through the grid-connected mode operation of ESS at a profile with no PV output, although all loads were restored with only OLTC tap control. In scenario 2, the amount of control was reduced maximally with the reactive

power output of PV and ESS when PV generates power. In scenario 3, the switch operation was reduced through the intentional islanding mode of ESS if it had enough energy to restore the unfaulty area. In scenario 4, the amount of control was reduced and more loads were restored when multiple faults were occurred through ESS operation. Also, it can be seen that both modes were simultaneously applied through proposed constraints of radiality and operation voltage range.

VI. CONCLUSION

In this study, an MILP-based SR method that utilized the operation of the existing infrastructure and the control of the DERs was proposed. For this purpose, linear constraints were formulated for the tap operation of the OLTCs, reactive power control of the DGs, and both grid-connected and intentional islanding operation of the ESSs, in addition to the existing switching operations and LS. The proposed method was formulated to consider the 15 min interval profiles of the load and PV. Simulation studies using a 150-node test system confirmed that the amount of LS and the number of switching and tap control operations decreased when the DERs were used in the SR process. In particular, the reactive power support of the PVs could alleviate the voltage violations; therefore, more loads could be restored, whereas the number of OLTC tap operations was decreased. The ESSs also helped to resolve the voltage issues regardless of the stored energy. When the SoC was sufficient, the ESSs could help to restore more loads and/or reduce the number of switching operations. If an ESS was installed in a section where the loads could not be transferred to other feeders, it could help to restore the loads in that area. Finally, the simulation of multiple faults confirmed that the proposed SR formulation could simultaneously deal with ESS operations in both grid-connected and islanding modes.

REFERENCES

[1] A. Angioni, A. Kulmala, D. D. Giustina, and M. Mirz, "Design and implementation of a substation automation unit," *IEEE Trans. Power Del.*, vol. 32, no. 2, pp. 1133–1142, Apr. 2017.

[2] M. S. Tsai, "Development of an object-oriented service restoration expert system with load variations," *IEEE Trans. Power Syst.*, vol. 23, no. 1, pp. 219–225, Feb. 2008.

[3] K. N. Miu, H.-D. Chiang, and R. J. McNulty, "Multi-tier service restoration through network reconfiguration and capacitor control for large-scale radial distribution networks," in *Proc. 21st Int. Conf. Power Ind. Comput. Appl. Connecting Utilities PICA Millennium Beyond*, May 1999, pp. 153–159.

[4] S. Dimitrijevic and N. Rajakovic, "Service restoration of distribution networks considering switching operation costs and actual status of the switching equipment," *IEEE Trans. Smart Grid*, vol. 6, no. 3, pp. 1227–1232, May 2015.

[5] M. Zadsar, M. Haghifam, and S. M. M. Larimi, "Approach for self-healing resilient operation of active distribution network with microgrid," *IET Gener., Transmiss. Distrib.*, vol. 11, no. 18, pp. 4633–4643, Dec. 2017.

[6] Y. Kumar, B. Das, and J. Sharma, "Multiobjective, multiconstraint service restoration of electric power distribution system with priority customers," *IEEE Trans. Power Del.*, vol. 23, no. 1, pp. 261–270, Jan. 2008.

[7] L. Tolomeu Marques, A. Claúdio B. Delbem, and J. B. Augusto London, "Service restoration with prioritization of customers and switches and determination of switching sequence," *IEEE Trans. Smart Grid*, vol. 9, no. 3, pp. 2359–2370, May 2018.

[8] A. Sharma, D. Srinivasan, and A. Trivedi, "A decentralized multiagent system approach for service restoration using DG islanding," *IEEE Trans. Smart Grid*, vol. 6, no. 6, pp. 2784–2793, Nov. 2015.

[9] A. Sharma, D. Srinivasan, and A. Trivedi, "A decentralized multi-agent approach for service restoration in uncertain environment," *IEEE Trans. Smart Grid*, vol. 9, no. 4, pp. 3394–3405, Jul. 2018.

[10] D. S. Popovic and Z. N. Popovic, "A risk management procedure for supply restoration in distribution networks," *IEEE Trans. Power Syst.*, vol. 19, no. 1, pp. 221–228, Feb. 2004.

[11] S. Khushalani, J. M. Solanki, and N. N. Schulz, "Optimized restoration of unbalanced distribution systems," *IEEE Trans. Power Syst.*, vol. 22, no. 2, pp. 624–630, May 2007.

[12] R. Romero, J. F. Franco, F. B. Leao, M. J. Rider, and E. S. de Souza, "A new mathematical model for the restoration problem in balanced radial distribution systems," *IEEE Trans. Power Syst.*, vol. 31, no. 2, pp. 1259–1268, Mar. 2016.

[13] P. L. Cavalcante, J. C. Lopez, J. F. Franco, M. J. Rider, A. V. Garcia, M. R. R. Malveira, L. L. Martins, and L. C. M. Direito, "Centralized self-healing scheme for electrical distribution systems," *IEEE Trans. Smart Grid*, vol. 7, no. 1, pp. 145–155, Jan. 2016.

[14] K. Chen, W. Wu, B. Zhang, and H. Sun, "Robust restoration decision-making model for distribution networks based on information gap decision theory," *IEEE Trans. Smart Grid*, vol. 6, no. 2, pp. 587–597, Mar. 2015.

[15] X. Chen, W. Wu, and B. Zhang, "Robust restoration method for active distribution networks," *IEEE Trans. Power Syst.*, vol. 31, no. 5, pp. 4005–4015, Sep. 2016.

[16] J. C. Lopez, J. F. Franco, M. J. Rider, and R. Romero, "Optimal restoration/maintenance switching sequence of unbalanced three-phase distribution systems," *IEEE Trans. Smart Grid*, vol. 9, no. 6, pp. 6058–6068, Nov. 2018.

[17] Z. Wang and J. Wang, "Self-healing resilient distribution systems based on sectionalization into microgrids," *IEEE Trans. Power Syst.*, vol. 30, no. 6, pp. 3139–3149, Nov. 2015.

[18] B. Chen, C. Chen, J. Wang, and K. L. Butler-Purry, "Multi-time step service restoration for advanced distribution systems and microgrids," *IEEE Trans. Smart Grid*, vol. 9, no. 6, pp. 6793–6805, Nov. 2018.

[19] B. Chen, C. Chen, J. Wang, and K. L. Butler-Purry, "Sequential service restoration for unbalanced distribution systems and microgrids," *IEEE Trans. Power Syst.*, vol. 33, no. 2, pp. 1507–1520, Mar. 2018.

[20] O. Bassey, K. L. Butler-Purry, and B. Chen, "Dynamic modeling of sequential service restoration in islanded single master microgrids," *IEEE Trans. Power Syst.*, vol. 35, no. 1, pp. 202–214, Jan. 2020.

[21] B. Chen, Z. Ye, C. Chen, and J. Wang, "Toward a MILP modeling framework for distribution system restoration," *IEEE Trans. Power Syst.*, vol. 34, no. 3, pp. 1749–1760, May 2019.

[22] M. Song, R. R. Nejad, and W. Sun, "Robust distribution system load restoration with time-dependent cold load pickup," *IEEE Trans. Power Syst.*, vol. 36, no. 4, pp. 3204–3215, Jul. 2021.

[23] N. C. Koutsoukis, P. S. Georgilakis, and N. D. Hatziargyriou, "Service restoration of active distribution systems with increasing penetration of renewable distributed generation," *IET Gener., Transmiss. Distrib.*, vol. 13, no. 14, pp. 3177–3187, Jul. 2019.

[24] W. Wu, Z. Tian, and B. Zhang, "An exact linearization method for OLTC of transformer in branch flow model," *IEEE Trans. Power Syst.*, vol. 32, no. 3, pp. 2475–2476, May 2017.

[25] *IEEE Standards Association*, IEEE Standard 1547, 2018.

[26] S. Guo, J. Lin, Y. Zhao, L. Wang, G. Wang, and G. Liu, "A reliability-based network reconfiguration model in distribution system with DGs and ESSs using mixed-integer programming," *Energies*, vol. 13, no. 5, p. 1219, Mar. 2020.

[27] Y. Zhang and A. Srivastava, "Voltage control strategy for energy storage system in sustainable distribution system operation," *Energies*, vol. 14, no. 4, p. 832, Feb. 2021.

[28] H. Abniki, S. M. Taghvaei, and S. M. Mohammadi-Hosseininejad, "Reliability improvement in smart grid through incorporating energy storage systems in service restoration," *Int. Trans. Electr. Energy Syst.*, vol. 29, no. 1, p. e2661, Jan. 2019.

[29] J. H. Choi, "Mid-to-long term operation plan of distribution control center according to expansion of distribution system intelligent equipment," KEPCO, Naju-si, South Korea, Final Rep., Dec. 2017, pp. 14–38.

[30] H. Ahmadi and J. R. Marti, "Linear current flow equations with application to distribution systems reconfiguration," *IEEE Trans. Power Syst.*, vol. 30, no. 4, pp. 2073–2080, Jul. 2015.

[31] M. S. Calovic, "Modeling and analysis of under-load tap-changing transformer control systems," *IEEE Trans. Power App. Syst.*, vol. PAS-103, no. 7, pp. 1909–1915, Jul. 1984.
[32] General Standard of KEPCO, *154 kV High Efficiency Power Transformers*, Standard GS-6120-0028, 2019.
[33] Y. Wang, Y. Xu, J. Li, J. He, and X. Wang, "On the radiality constraints for distribution system restoration and reconfiguration problems," *IEEE Trans. Power Syst.*, vol. 35, no. 4, pp. 3294–3296, Jul. 2020.
[34] C. Y. Park and C. S. Huh, "Assessment of customer interruption cost by regional groups for macro approach," *J. Korean Inst. Illum. Elect. Installation Eng.*, vol. 19, no. 1, pp. 124–129, Jan. 2005.
[35] Y. S. Nam and J. Y. Lee, "Study on optimal trading method of REC by solar power generation," *Environ. Resource Econ. Rev.*, vol. 29, no. 1, pp. 91–111, Mar. 2020.
[36] I. K. Hwang, Y. G. Jin, Y. T. Yoon, and J. B. Choo, "Determining the reference voltage of 345 kV transmission system considering economic dispatch of reactive power," *Trans. Korean Inst. Elect. Eng.*, vol. 67, no. 5, pp. 611–616, Mar. 2018.

MI-GON CHOI (Student Member, IEEE) received the B.S. and M.S. degrees in electrical engineering from Chonnam National University, South Korea, in 2015 and 2017, respectively, where he is currently pursuing the Ph.D. degree with the Electrical Engineering Department. His research interests include the adaptive protection and restoration of active distribution networks.

JOON-HO CHOI (Senior Member, IEEE) received the B.S., M.S., and Ph.D. degrees in electrical engineering from Soongsil University, Seoul, South Korea, in 1996, 1998, and 2002, respectively. Since 2003, he has been a Professor at Chonnam National University, Gwangju, South Korea. His research interests include operation and integration and control strategies of distributed generation, distribution automation, and modeling and operation algorithms of the smart grid. He is a Life Member of the KIEE and the Korean Institute of Illuminating and Electrical Installation Engineers and a Committee Member of IBS, South Korea. Since 2004, he has been an Associate Editor of the Transactions of the KIEE.

SANG-YUN YUN received the B.S., M.S., and Ph.D. degrees in electrical engineering from Soongsil University, Seoul, South Korea, in 1996, 1998, and 2002, respectively. From 2002 to 2009, he was a Senior Researcher at the Electrotechnology Research and Development Center, LS Industrial Systems, Cheongju, South Korea. From 2009 to 2016, he was a Principle Researcher at the KEPCO Research Institute, Daejeon, South Korea. He is currently an Associate Professor at the Department of Electrical Engineering, Chonnam National University, Gwangju, South Korea. His current research interests include the design of EMS, DMS, and MG operation systems, protection technologies for active distribution networks, and the application of PMUs in power distribution networks.

SEON-JU AHN (Member, IEEE) received the B.S., M.S., and Ph.D. degrees in electrical engineering from Seoul National University, Seoul, South Korea, in 2002, 2004, and 2009, respectively. He was a Postdoctoral Researcher at Myongji University, Seoul, and the FREEDM Systems Center, North Carolina State University, Raleigh, NC, USA. He is currently an Associate Professor at Chonnam National University, Gwangju, South Korea. His current research interests include power quality, distributed energy resources, microgrids, smart grids, and real-time simulation.